Resonantly enhanced multiphoton ionization of krypton and xenon with intense ultraviolet laser radiation

Michael D. Perry and Otto L. Landen
Lawrence Livermore National Laboratory, University of California, P.O. Box 808, Livermore, California 94550
(Received 22 February 1988)

The absolute yield of singly and multiply charged ions of krypton and xenon and resulting photoelectron spectra produced by intense laser radiation in the range 285–310 nm are presented. Enhancement of the yield of Kr^+ by two orders of magnitude in the vicinity of the $4p^5 4d$ and $4p^5 4d'$ manifolds is observed at intensities exceeding 10^{13} W/cm^2. These observations extend the intensity at which strong resonant enhancement has been observed in multiphoton ionization by two orders of magnitude. A model incorporating line shifts and linewidths scaling linearly with intensity is in good agreement with the experimental results. Absolute cross sections for multiphoton ionization of xenon and krypton are presented and compared with recent theoretical calculations.

I. INTRODUCTION

Resonantly enhanced multiphoton ionization (REMPI) has been the subject of extensive experimental[1–6] and theoretical[1,7–10] interest since the invention of the laser. These investigations have led to some interesting and practical applications in spectroscopy.[5,11,12] To date, the overwhelming majority of REMPI studies have been conducted at what may now be considered modest intensities, $I < 10^{11}$ W/cm^2. At these intensities, the magnitude of the applied laser field remains less than 1% of the atomic Coulomb field experienced by the outer electrons in a typical rare-gas atom. In this regime, the treatment of the applied field as simply a weak perturbation on the atomic system should yield an accurate theoretical description of the experimental observations. Indeed, in those few cases where complete perturbation-theory calculations have been possible, the theoretical calculations have been in excellent agreement with the experimental results.[13] For multielectron atoms, complete perturbation-theory calculations are just now being attempted.[14] Nevertheless, most of the qualitative features of both resonant and nonresonant multiphoton ionization of the rare gases at modest intensities can be explained within the framework of perturbation theory.

The work described here investigates resonant enhancement of the multiphoton ionization probability at much higher laser intensities, specifically, to examine the behavior of multiphoton resonances as the strength of the applied field approaches that of the atomic Coulomb field. In this regime, it may no longer be adequate to treat the applied field as merely a perturbation on the atomic system.

Such an investigation requires laser intensities exceeding 10^{13} W/cm^2. At intensities this high, the shifts and widths of the intermediate atomic levels are expected to be large, prompting some to suggest that resonant enhancement could no longer be observed.[15] Indeed, no resonant enhancement of the multiphoton ionization of krypton at 10^{13} W/cm^2 was observed in an earlier experiment.[16] However, tentative evidence of resonance structure in the multiphoton ionization of xenon has been reported at 3×10^{13} W/cm^2.[17]

The experiments described here were also motivated by the extremely large difference in the absolute magnitude of the theoretical calculations for the ionization rates of the noble gases. A perturbation-theory calculation using multichannel quantum-defect theory[14] predicts an ionization rate of 8×10^{18} sec^{-1} for xenon at an intensity of 2×10^{13} W/cm^2 and 293 nm, while a time-dependent Hartree-Fock calculation predicts an ionization rate of 2×10^{12} sec^{-1}.[18] These calculations differ by nearly seven orders of magnitude.

In this paper, we present detailed spectral profiles of the three-photon resonant, four-photon ionization of krypton in the region 285–310 nm. The intensity at the laser focus was varied from 3×10^{12} to 10^{14} W/cm^2 and was accurately determined using a technique based on the shift of the energy of photoelectrons produced in multiphoton ionization by a "short" laser pulse.[19] To our knowledge, these are the first observations of significant resonant enhancement in the multiphoton ionization of the noble gases at intensities exceeding 10^{13} W/cm^2. Measurements of the ac Stark shift and photoionization cross sections of some of the $4d$ and $4d'$ intermediate states are presented along with measurements of the absolute cross sections for multiphoton ionization of both Kr and Xe at 288.5, 293.0, and 298.0 nm.

II. EXPERIMENT

A. Method

The experiments consisted of measuring the number of singly and multiply charged ions of krypton and xenon as a function of both laser frequency and intensity. The location of the resonances and the laser intensity determined in the ion yield measurements were then confirmed

by measuring the yield and energy distributions of photoelectrons produced in the four-photon ionization of krypton (Sec. II B).

The emphasis on measuring the absolute yield of ions of each charge state was dictated by the desire to obtain absolute measurements of multiphoton ionization cross sections and excitation rates to intermediate states. In these experiments, such information cannot be obtained accurately by the technique of measuring the "saturation intensity."[20] This is due to the fact that for multiphoton processes of nonlinear order less than approximately 5, the transition between the unsaturated and saturated regimes in the ion yield is too gradual to be accurately determined.

Details of the laser system have been described elsewhere.[21] Briefly, the laser system consists of a well-diagnosed, amplified, synchronously mode-locked dye laser. The dye laser oscillator is pumped by the second-harmonic output of a cw mode-locked Nd:YAG (yttrium aluminum garnet) laser operating at 82 MHz with an average power of 1.2 W at 532 nm. The pulse length of the dye laser can be adjusted from 0.6 to 6 psec by cavity tuning and/or addition of small amounts of a saturable absorber to the dye jet. Frequency tuning is accomplished through the use of a two-plate birefringent filter placed internal to the cavity. The output of the dye laser oscillator is amplified in a five-stage amplifier which is pumped by the second-harmonic output of a Q-switched Nd:YAG laser operating at a repetition rate of 1–10 Hz. The system provides pulses which are continuously tunable over the range 570–620 nm. Pulse energies are typically 3 mJ with an approximately 10% amplified spontaneous emission component centered at 583 nm and lasting 2 nsec in duration. The pulses are Fourier-transform–limited ($\Delta\nu\,\Delta\tau=0.29\pm0.04$), of which approximately 80% of the energy is in the lowest-order spatial mode. For the experiments considered here, this output is frequency doubled in a 1-cm-thick potassium dihydrogen phosphate crystal (KDP) to a maximum pulse energy of 0.8 mJ which is continuously tunable from 285 to 310 nm. The laser energy is measured on every shot using a calibrated vacuum photodiode.

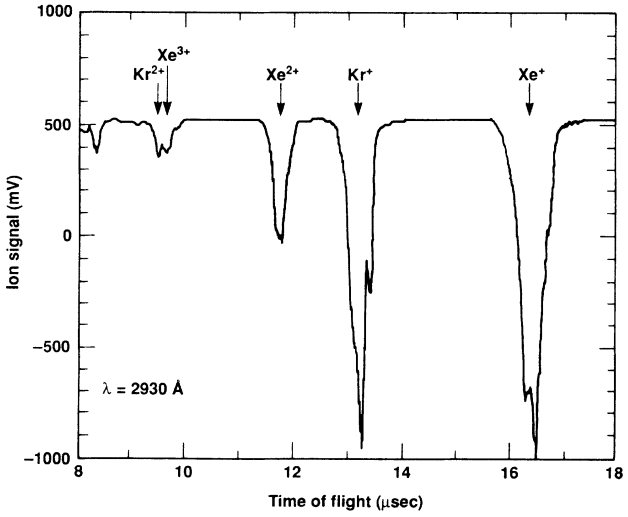

FIG. 1. Time-of-flight ion spectrum for mixed krypton and xenon target ($P_{\mathrm{Kr}}=P_{\mathrm{Xe}}=1.6\times10^{-6}$ Torr) at 293 nm and a peak intensity of 1×10^{14} W/cm^2 (laser pulse width $T_p=1.5$ psec).

The linearly polarized uv beam is separated from the remaining fundamental by a fused-silica prism and focused by an $f/15$ lens into an equal mixture of Kr and Xe gas at a pressure of 3×10^{-6} Torr. The ions are analyzed using a time-of-flight spectrometer which was designed with a resolution sufficient to completely resolve the isotope structure of natural xenon. A uniform electric field of 5000 V/cm applied across the interaction region extracts any ion produced at the laser focus. The ions are detected by direct impact on a 2.5-cm-diam microchannel plate. A second microchannel plate placed in a chevron configuration behind the first increases the gain to 10^{-6} e^-/ion. This system has the sensitivity to readily detect single ions. A typical time-of-flight spectrum is shown in Fig. 1.

The intensity distribution at the focus was determined to be separable into a product of purely spatial and temporal distributions. The temporal distribution of the ultraviolet pulse was determined by cross correlation with the fundamental pulse and found to be well described by a hyperbolic secant squared distribution of 1.3 psec width for a fundamental input pulse of 1.5 psec. The spatial distribution was found to be nearly Gaussian with a $1/e^2$ radius at the focus of 12.5 μm. The complete distribution is well described by

$$I(r,t)=I_0\frac{\mathrm{sech}^2(2t/T_p)}{1+(\beta\lambda z/\pi w_0^2)^2}\times\exp\left[-\frac{2r^2}{w_0^2[1+(\beta\lambda z/\pi w_0^2)^2]}\right], \quad (1)$$

where w_0 is the $1/e^2$ radius at the focus and β is an empirically determined constant to account for a divergence rather than diffraction-limited focus. In these experiments $\beta=4.5$. The pulse width T_p is defined as the integral of the temporal distribution and is related to the full width at half maximum by

$$T_p=\int_{-\infty}^{\infty}T(t)dt=1.14T_{\mathrm{FWHM}}\ , \quad (2)$$

where $T(t)=\mathrm{sech}^2(2t/T_p)$. The peak intensity I_0 is defined as the intensity at $r=z=t=0$ and is determined from laser pulse measurements as $I_0=2E/(T_p\pi w_0^2)$, where E is the pulse energy.

B. Determination of the absolute laser intensity via ponderomotive energy shifts

A technique for determining the local laser intensity by measuring the energy distribution of photoelectrons produced by a short laser pulse is described elsewhere.[19] The technique is based on the shift of the electron energy from its field-free value by the ponderomotive potential present at the laser focus.[22] Specifically, the kinetic energy of an electron produced as the result of an atom absorbing K photons of energy $\hbar\omega$ is given approximately by

$$E_e=K\hbar\omega-I_p(0)-U_p(\mathbf{r},t)\ , \quad (3)$$

where $I_p(0)$ is the ionization potential of the atom in the absence of the field, and $U_p(\mathbf{r},t)=9.33\times10^{-14}I(\mathbf{r},t)\lambda^2$ is the ponderomotive potential, $I(\mathbf{r},t)$ is the local laser intensity in W/cm^2, and λ is the wavelength of the laser light in microns.

If the duration of the laser pulse is less than the time required for the electron to leave the laser focus, the ponderomotive potential and hence the laser intensity can be determined by measuring the shift in kinetic energy of the electron from its field-free value.[23–25] The short pulse regime can be realized with lasers producing picosecond or subpicosecond pulses. For example, a 4-eV electron travels less than 1.2 μm during a 1-psec pulse. This is only 6% of a typical 20-μm-diam laser focus. This small motion during the laser pulse should be included in a precise calculation of the electron energy distribution and will modify the relation between the electron energy and laser intensity given in Eq. (3).[17,23,25] For the experiments described herein, the error associated with the intensity measurement as a result of neglecting the electron motion is less than 10%.

The electron spectrometer used in these experiments is a magnetic-bottle type first described by Kruit and Read.[26] The spectrometer collects all electrons emitted in the 2π direction of the microchannel plate detector. The energy of a given photoelectron is determined by its time of flight down a 50-cm drift tube. A typical spectrum resulting from the above-threshold ionization (ATI) of xenon at 293 nm is shown in Fig. 2.

The spectrometer was calibrated using two different methods. The first involved the above-threshold ionization of xenon at 532 nm using long (70-psec) laser pulses at an intensity of approximately 10^{13} W/cm^2. The resulting electron spectrum exhibits several ATI peaks, each located at an energy which is given by the difference between the number of photons absorbed and the field-free ionization potential. The peaks are unshifted from their field-free positions as the long duration of the laser pulse is sufficient for all of the electrons to leave the focal volume during the pulse.[27]

The second calibration method involved utilizing resonantly enhanced multiphoton ionization of krypton with our short (1-psec) pulses. By utilizing the strong resonant enhancement near 288.5 nm (see Sec. III), it was possible to produce electron signals corresponding to both the $P_{3/2}$ and $P_{1/2}$ core states (Fig. 3) at intensities below 5×10^{12} W/cm^2. At these intensities and frequency, the value of the ponderomotive potential was below 40 meV, resulting in a negligible shift of the electron energies from the field-free values. The energy separation of the peaks (670 meV) and their positions corresponding to $4\hbar\omega-I_p(0)$ at 3.19 and 2.52 eV, respectively, serve as absolute energy values for calibration.

The experiments to determine the absolute laser intensity present at the laser focus were conducted in a range of pressure from 4×10^{-8} to 5×10^{-6} Torr. The pressure was decreased as the laser intensity was increased so as to maintain electron signals of approximately constant amplitude. In all cases, the number of ions being produced was kept sufficiently low so that distortion of the electron energy distribution due to space-charge effects[28] was negligible. The laser wavelength was tuned to 293 nm in an effort to avoid any intermediate three-photon resonances. In separate experiments conducted in the visible, the effect of intermediate resonances leading to significant structure in both the threshold and above-threshold peaks has been observed.[17,29]

Some of the electron spectra for krypton at 293 nm are shown in Fig. 4. The shift of the position of the peaks towards lower energy with increasing laser intensity is clearly observable. In Fig. 5, the shifts of the peaks from their field-free positions are plotted as a function of peak laser intensity as determined from separate measurements of laser pulse parameters. The shift of the peak exhibits a linear dependence on laser intensity. The energy shift of

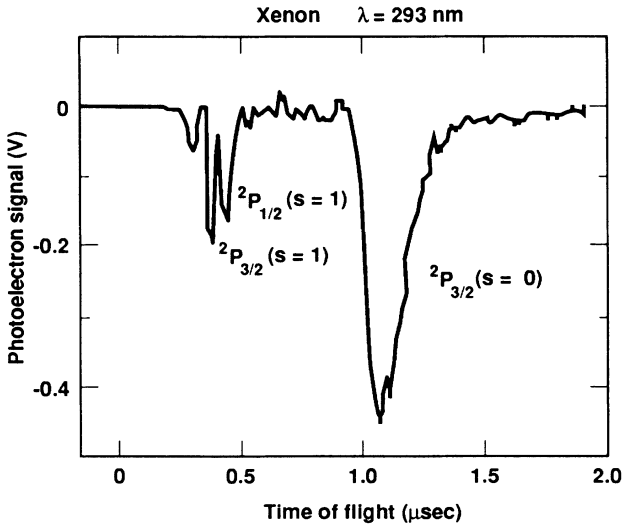

FIG. 2. Typical time-of-flight photoelectron spectrum resulting from the multiphoton ionization of xenon at 293 nm and a peak intensity of approximately 4×10^{13} W/cm^2. Electrons corresponding to above-threshold ionization ($s=1,2$) are evident.

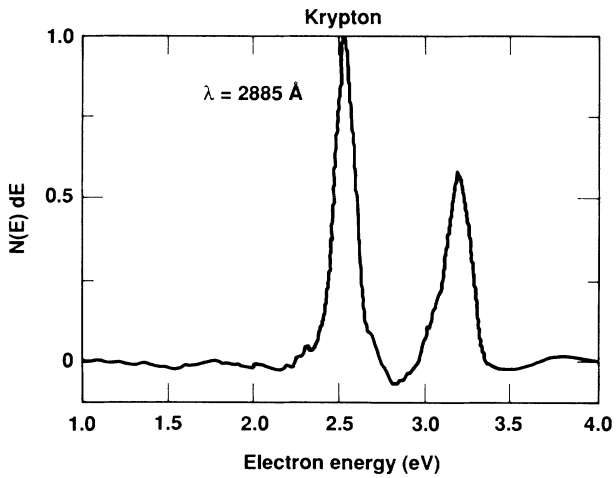

FIG. 3. Electron spectra from the three-photon resonant, four-photon ionization of krypton at 288.5 nm and a peak intensity of 4×10^{12} W/cm^2. The signals at 3.2 and 2.5 eV correspond to the $^2P_{3/2}$ and $^2P_{1/2}$ ground states of Kr^+, respectively.

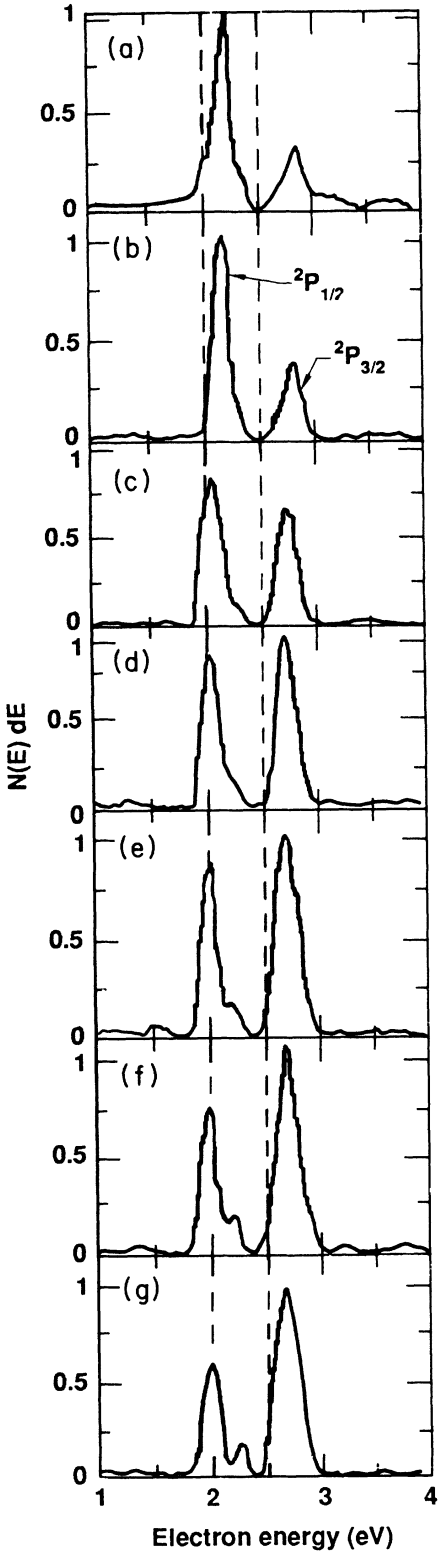

FIG. 4. Electron spectra from four-photon ionization of krypton at 293 nm at selected peak intensities (10^{13} W/cm^2): (a) 0.9, (b) 1.63, (c) 3.3, (d) 4.1, (e) 5.9, (f) 8.0, (g) 12.0 (laser pulse width $T_p = 1.3$ psec).

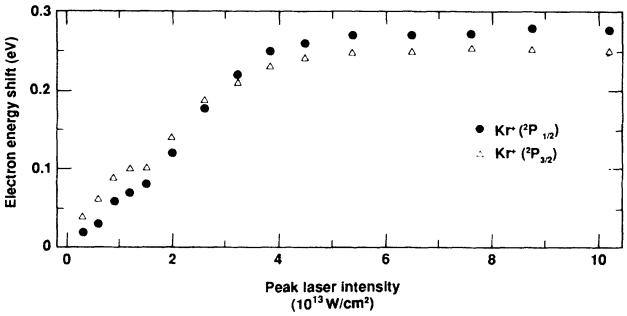

FIG. 5. Shift of the *peak* of the electron energy distribution as a function of peak laser intensity ($T_p = 1.3$ psec).

the peak of the distribution represents the most probable intensity for ionization, and not the peak laser intensity present. A calculation of the laser intensity based on the shifts in Fig. 5 must be corrected by the ratio of the most probable intensity for ionization to the peak laser intensity (for these experiments, this ratio is 0.68).[19] It is satisfying to note that the value of the laser intensity obtained using this technique is within 20% of that obtained by the conventional method involving separate measurements of the pulse energy, width, and spatial distributions.

Eventually, *no further shift is observed, indicating saturation of the ionization probability.*[24] The saturation intensity for the four-photon ionization of krypton at 293 nm is readily observable in Fig. 5 as 4.5×10^{13} W/cm^2.

III. EXPERIMENTAL RESULTS

A. Ionization of xenon

Over the range of intensity investigated, the yield of Xe^+ exhibited no discernible resonant enhancement between 285 and 300 nm (Fig. 6). This observation is in contrast to the results of Pratt *et al.*,[30] who observed weak three-photon autoionizing resonances between the $P_{1/2}$ and $P_{3/2}$ fine-structure ionization thresholds of Xe in the range 280–290 nm. The results of the two experiments are not in conflict, however, since the experiments of Pratt *et al.* were performed at much lower values of laser intensity ($I \leq 3 \times 10^{10}$ W/cm^2). An extrapolation of

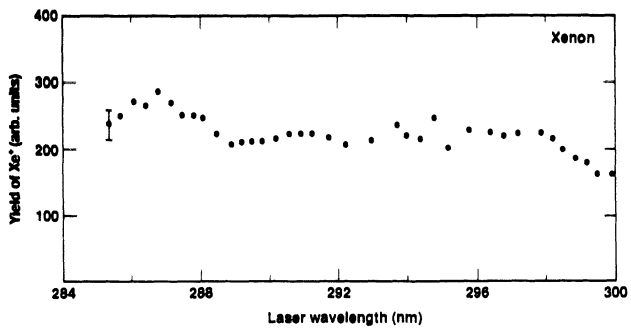

FIG. 6. Relative yield of Xe^+ as a function of laser wavelength at a peak intensity of 2×10^{13} W/cm^2.

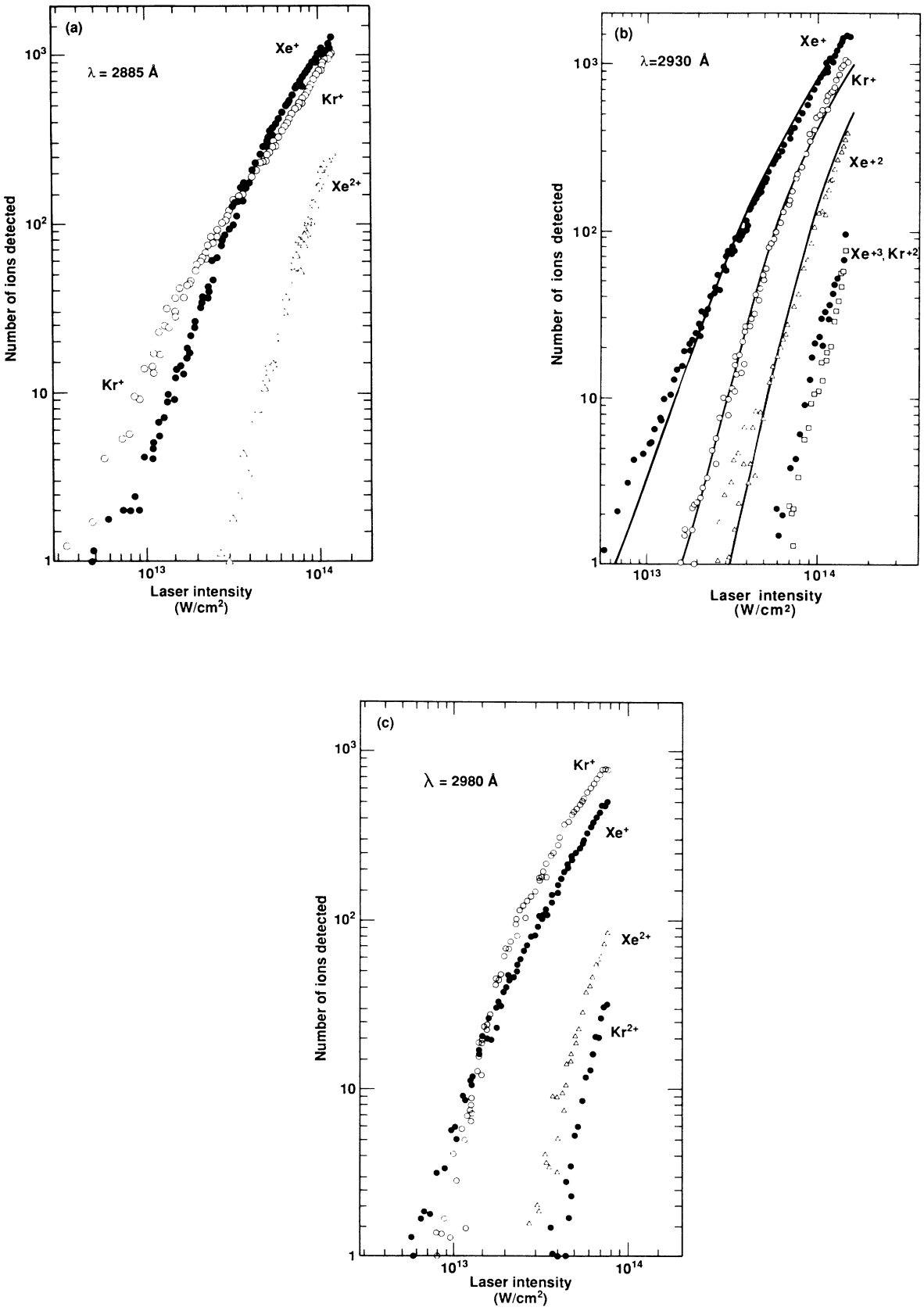

FIG. 7. Absolute ion yield of krypton ($P_{Kr}=1.4\times10^{-6}$ Torr) and xenon ($P_{Xe}=1.6\times10^{-6}$ Torr) as a function of peak laser intensity at selected laser frequencies: (a) 288.5 nm, near resonance *B* of Fig. 10; (b) 293 nm, nonresonant; (c) 298 nm, near resonance *C*.

their results to the intensities considered here suggests that such resonances associated with the $P_{1/2}$ core would be completely merged with the three-photon nonresonant ionization to the $P_{3/2}$ core state of Xe^+. The fact that the Xe^+ signal exhibited no resonance behavior made it possible to use this signal as an additional diagnostic to determine the intensity at which the multiply charged ions of krypton were produced. This was accomplished by measuring the production of multiply charged xenon and krypton ions simultaneously.

The absolute yield of multiply charged xenon ions was studied as a function of intensity at several selected wavelengths, both to confirm the general lack of resonance structure and to determine values for the cross section $\sigma^{(K)}$. The ion yield at three of these frequencies is shown as a function of peak laser intensity in Fig. 7. Although there is clear evidence of resonant behavior in the Kr^+ yield, the yield of both Xe^+ and Xe^{2+} is essentially independent of wavelength. The curvature in the ion yield curves for the singly charged ions above approximately 3×10^{13} W/cm^2 is due to saturation of the ionization probability. Specifically, as the ionization probability approaches unity, the target atoms become depleted throughout the focal volume. Further contribution to the ion yield then comes from the expanding focal volume which grows as $I_0^{3/2}$.[21,31]

The production of multiply charged ions of both krypton and xenon was analyzed using a kinetic model developed previously.[21] The model includes both direct and sequential ionization leading to the production of the higher charge states. However, as in the case of earlier experiments,[21,32,33] no evidence is found here to suggest a significant contribution of direct processes to the formation of Kr^{2+}, Xe^{2+}, or Xe^{3+}.

As neither the yield of Xe^+ nor Xe^{2+} exhibits any evidence of resonant enhancement, we have used the nonresonant ionization rate predicted by lowest-order perturbation theory, $W(\mathbf{r},t)=\sigma^{(K)}I^K(\mathbf{r},t)$, to model the experimental results. The value of the cross section was varied to provide the best agreement between the experimental ion yield and that predicted by the model. All other parameters were held fixed at their experimentally measured values. The results of these calculations are shown as the solid curves in Fig. 7(b). The corresponding cross sections are given in Table I.

The cross section for the three-photon ionization of neutral xenon can be compared with the theoretical values of Gangopadhay *et al.*[14] and Kulander.[18] Although a factor of 3 below that of Kulander, such agreement should be considered excellent considering the complexity of the calculation. Furthermore, the experimental results suggest a clear problem with the magnitude of the earlier calculation by Gangopadhay. (An error has recently been discovered in this calculation and the revised results are close to our experimental value.[34])

These results may also be reported in terms of the saturation intensity mentioned earlier. The relationship between the saturation intensity and the cross section $\sigma^{(K)}(\omega)$ is defined by the rate expression for the number of ions produced,

$$N(\omega,I_0)=\int_{-\infty}^{\infty} n_0(\mathbf{r},-\infty)\left[1-\exp\left[-\sigma^{(K)}(\omega)I_0^K F^K(\mathbf{r})\int_{-\infty}^{\infty}T^K(t)dt\right]\right]d^3\mathbf{r}\ , \tag{4}$$

where we have assumed a separable intensity distribution $I(\mathbf{r},t)=I_0F(\mathbf{r})T(t)$ and an ionization rate $W(\omega,\mathbf{r},t)=\sigma^{(K)}(\omega)I^K(\mathbf{r},t)$. The saturation intensity is defined as the intensity at the spatial peak of the pulse ($F=1$) for which the argument of the exponential reaches unity,

$$\sigma^{(K)}(\omega)I_{\rm sat}^K T_p^{(K)}=1\ , \tag{5}$$

where $T_p^{(K)}$ is the integral over $T^K(t)$ in Eq. (4). Measurements of the Kth-order cross section and the saturation intensity are equivalent, provided $T_p^{(K)}$ can be determined. For our hyperbolic secant squared distribution, this Kth-order pulse width is given by

$$T_p^{(K)}=2^{K-1}\frac{(K-1)!}{(2K-1)!!}T_p\ , \tag{6}$$

where T_p is defined in Eq. (2).

It is clear from the agreement between our model calculations and the data in Fig. 7 that, in the case of xenon, the general features of the ionization probability are accurately described by a rate proportional to the third power of the local laser intensity for the values of laser frequency and intensity considered here. The influence of "tunneling" ionization and the effect of above-threshold ionization apparent in Fig. 8 are discussed in Sec. IV.

The energy spectrum of the photoelectrons resulting

TABLE I. Multiphoton ionization cross sections.

Species	Number of photons	Cross section ($cm^{2K}\,sec^{K-1}$)	Saturation intensity (W/cm^2)
Xe	3	$(2\pm1)\times10^{-83}$[a]	3×10^{13}
Kr	4	$(8\pm4)\times10^{-116}$	4.5×10^{13}
Xe^+	6	$(5\pm3)\times10^{-180}$	5.8×10^{13}

[a]Theoretical values: Kulander (Ref. 18) is 7×10^{-83} cm^6 sec^2, Gangopadhay *et al.* (Ref. 14) is 3×10^{-76} cm^6 sec^2.

from above-threshold ionization of xenon at 293 nm is shown in Fig. 8. At the lowest intensities, essentially all of the ions are produced in the $^2P_{3/2}$ ground state. This corresponds to the lowest-order pathway since an additional photon is required to produce an ion in the $^2P_{1/2}$ state (Fig. 9).

As the intensity is increased, production of the ion in the $^2P_{1/2}$ state can be observed along with the appearance of the first above-threshold peak ($s=1$) for the $^2P_{3/2}$ state. The intensity at which these four-photon processes occur is, within the experimental uncertainty, the same. Also, at the lowest intensities, the relative yield between these processes is very nearly the expected statistical ratio 2:1. Therefore, at the lowest intensities, it appears that the probability for above-threshold ionization and four-photon ionization to the $^2P_{2/1}$ core in xenon at 293 nm is, aside from statistical weighting, the same.

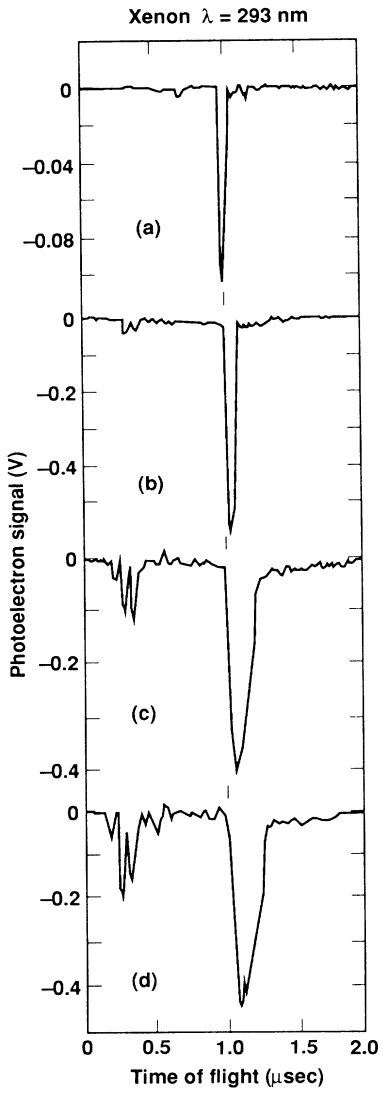

FIG. 8. Photoelectron time-of-flight spectra resulting from the above-threshold ionization of xenon at 293 nm. Peak near 1 μsec corresponds to threshold ionization (Fig. 9). (a) $I_0 \approx 3\times10^{12}$ W/cm^2, $P_{Xe}=3\times10^{-6}$ Torr, (b) $I_0 \approx 2\times10^{13}$ W/cm^2, $P_{Xe}=3\times10^{-7}$ Torr, (c) $I_0 \approx 8\times10^{13}$ W/cm^2, $P_{Xe}=2\times10^{-8}$ Torr, and (d) $I_0 \approx 1\times10^{14}$ W/cm^2, $P_{Xe}=2\times10^{-8}$ Torr.

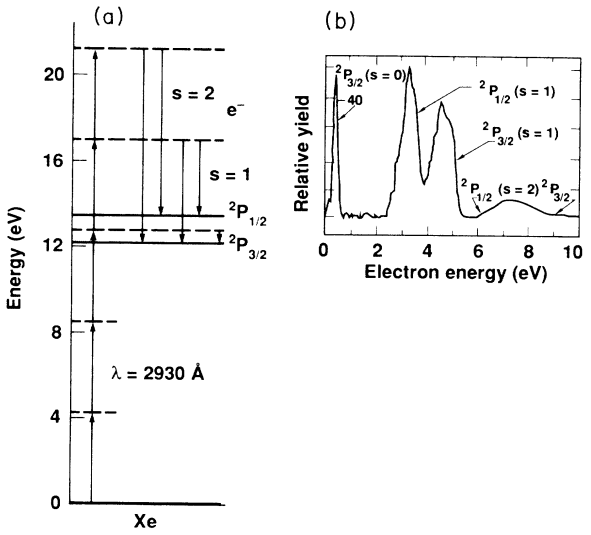

FIG. 9. (a) Energy-level diagram of Xe, (b) electron energy spectrum resulting from above-threshold ionization at 293 nm and a peak intensity of 1×10^{14} W/cm^2. Electron yield corresponding to one ($s=1$) and two ($s=2$) photons absorbed beyond the minimum required to ionize is evident. Threshold ($s=0$) peak has been divided by a factor of 40 to facilitate comparison with the above-threshold peaks.

As the intensity is increased further, the five-photon processes corresponding to $^2P_{3/2}(s=2)$ and $^2P_{1/2}(s=1)$ become observable. In addition, electrons near 1.27, 4.17, 5.5, and 8.4 eV are expected at the highest intensities resulting from production of Xe^{2+}. From the ion yield data in Fig. 7, the electron signal from Xe^{2+} should be approximately 10% of that from Xe^+ at peak intensities exceeding 10^{14} W/cm^2. Although the experiments here were not of sufficient resolution to make identification of these electrons unambiguous, the asymmetry in the peaks near 4.5 and 8 eV may be due to these Xe^{2+} electrons.

The suppression of the lowest-energy channel, observed first by Kruit *et al.*[27] in xenon at 1064 nm and later by many others,[35–38] is not expected to be observed in these experiments. At 293 nm, the laser intensity necessary to suppress threshold ionization ($s=0$) to the $^2P_{3/2}$ core state of xenon is 7×10^{13} W/cm^2 [Eq. (3)]. This is far above the measured saturation intensity of 3×10^{13} W/cm^2. The photoelectron yield should therefore be dominated by electrons associated with the absorption of three-photons. This is clearly observed in Figs. 8 and 9. In Fig. 9, the peak corresponding to threshold ionization has been divided by a factor of 40 relative to the above-threshold peaks. The effect of the ponderomotive potential on the energy spectrum is easily observed in Fig. 8 as a shift in the time of flight of the electrons. As the intensity increases, the kinetic energy of electrons leaving the laser focus decreases, resulting in an increase in the time of flight (Sec. II B).

B. Four-photon ionization of krypton

Resonant enhancement of the yield of singly charged krypton ions at 288.5 and 298.0 nm is readily apparent in Figs. 7(a) and 7(c), respectively. At 288.5 nm, the ionization probability of krypton is above that of xenon at low intensity, but falls below that of xenon at higher intensities. This behavior could be the result of the laser being initially resonant with an intermediate state. As the intensity is raised, the intermediate state is shifted out of resonance by the strong field. In contrast, at 298.0 nm, the Kr^+ yield starts out below the yield of Xe^+ but rises above the yield of singly charged xenon at an intensity of approximately 1.5×10^{13} W/cm^2. This could be the result of the strong field shifting the intermediate state into resonance. Finally, at 293 nm, the Kr^+ signal exhibits no evidence of significant resonant enhancement. At this frequency, the Kr^+ yield exhibits an $I^{4.0\pm0.3}$ dependence on the peak intensity which is consistent with nonresonant, four-photon ionization in the multiphoton regime.[39]

The yield of Kr^+ is shown as a function of laser wavelength in Fig. 10 for increasing laser intensity.[40] Each point represents the average of 30–60 laser shots at a given peak intensity. Several resonances are apparent. Reference to the krypton energy-level diagram given in Fig. 11 indicates that several intermediate states may be accessed by dipole-allowed, three-photon transitions over the range of laser frequency examined here.[41] The level designations are given in abbreviated $j_c l$ notation in which a prime is used to denote states with a $P_{1/2}$ core.

We have identified the intermediate states producing the resonant enhancement on the basis of an extrapolation of the position of the resonance to the limit of no applied field. In some cases, such an extrapolation does not yield an unambiguous identification, e.g., the $4d'[\frac{3}{2}]_1$ and the $5d[\frac{7}{2}]_3$. In these cases, identification has been made on the basis of estimates of the relative three-photon oscillator strengths (matrix elements). These third-order matrix elements were estimated using the "truncated summation" method[42] with published theoretical values of the single-photon matrix elements[43] connecting the states along the dominate pathway.

From these calculations and the extrapolated resonance positions, the intermediate states observed are

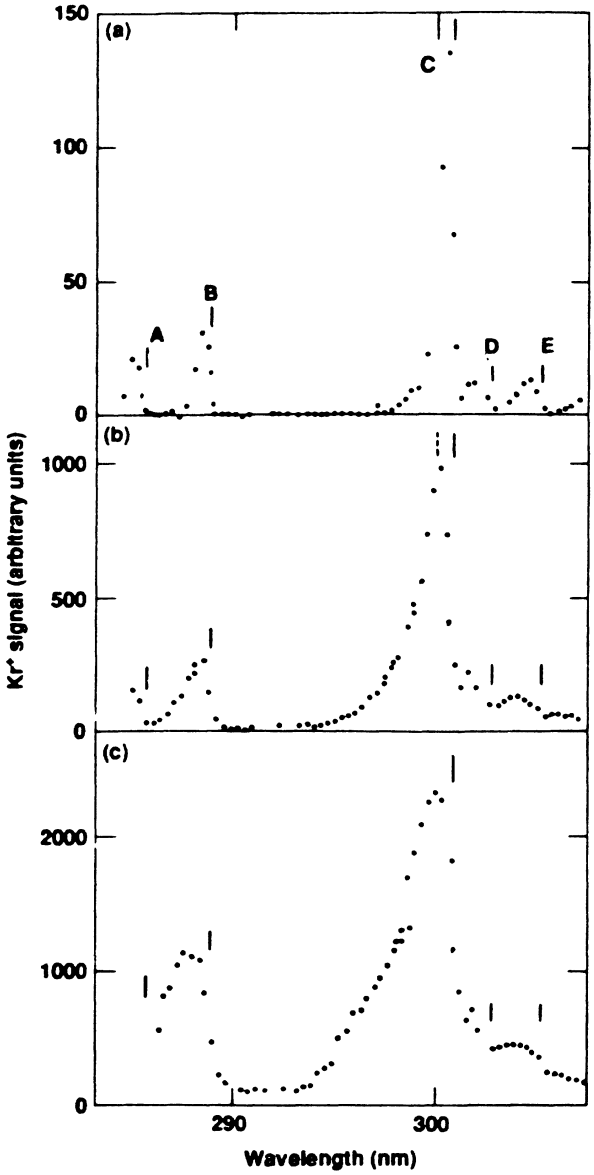

FIG. 10. Relative yield of singly charged krypton ions as a function of laser wavelength at various peak intensities: (a) $I_0=6\times10^{12}$ W/cm^2, (b) $I_0=1.4\times10^{13}$ W/cm^2, (c) 3×10^{13} W/cm^2. Vertical lines mark the field-free positions of dipole-allowed, three-photon resonances in neutral Kr (Fig. 11).

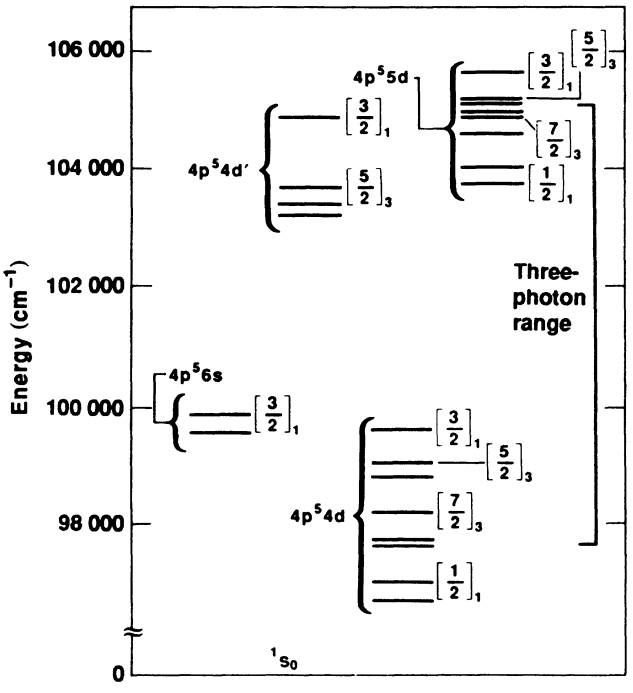

FIG. 11. Partial energy-level diagram of Kr I exhibiting states accessible by three laser photons. Only the three-photon, dipole-allowed $J=1$ and 3 states are labeled and correspond to the vertical lines in Fig. 10.

identified as A, which equals a combination of the $4d'[\frac{3}{2}]_1$ and the $5d[\frac{7}{2}]_3$; B, which equals a combination of the $4d'[\frac{5}{2}]_3$ and the $5d[\frac{1}{2}]_1$; C, which equals a combination of both the $4d[\frac{3}{2}]_1$ and $6s[\frac{3}{2}]_1$ (extrapolation of the resonance position suggests that the enhancement arises primarily from the state located at 99 646.3 cm^{-1}; however, a controversy exists in the literature regarding assignment of this state[41,43]); D, which equals $4d[\frac{5}{2}]_3$; E, which equals $4d[\frac{7}{2}]_3$; and F, which equals probably the $4d[\frac{1}{2}]_1$. It should be noted that configuration mixing among the $4d'$ and $5d$ states may be strong, making such single level designations invalid. Configuration mixing at low intensity in resonantly enhanced multiphoton ionization has been studied previously using photoelectron spectroscopy.[44,45] Furthermore, the estimates of the three-photon matrix elements and the level designations given above follow from knowledge of the wave functions in the absence of an applied field. In the case of strong applied fields, the coupling of the excited electron to the field can be stronger than the spin-orbit interactions which give rise to the level splittings and consequent coupling schemes. This is particularly true for the present experimental conditions. Therefore such level designations and strength estimates must be treated with caution.

As can be seen from Fig. 10, both the location and widths of the resonances shift and broaden with increasing laser intensity. Therefore, in order to study the nonresonant multiphoton ionization of krypton, a laser frequency must be chosen which is sufficiently far from resonance that the field-induced shifts and broadening are incapable of significantly affecting the ionization probability. This becomes increasingly difficult at large values of laser intensity.

At the lowest intensities, the region around 293 nm remains relatively unaffected by intermediate resonances and may therefore be used to determine a nonresonant four-photon ionization cross section. This cross section was determined using the same procedure as described previously for xenon. The solid curve in Fig. 7(b) illustrates the results of model calculations using the cross section given in Table I. As described in Sec. II, the saturation intensity can also be determined by measuring the shift of the energy of photoelectrons produced by a short laser pulse. The value of the saturation intensity measured for Kr at 293 nm using this technique was found to be within 20% of that determined from the value of the cross section obtained from the absolute ion yields.

At higher intensities, the strong resonance located near 300 nm begins to influence the ion yield at 293 nm. This observation is confirmed by the appearance of the electron spectra of Fig. 4. The electron spectra are initially dominated by electrons with kinetic energy corresponding to four-photon ionization to the $^2P_{1/2}$ core. At our lowest intensities, the ratio of electron yield to the $^2P_{1/2}$ to the $^2P_{3/2}$ is greater than 4:1, respectively. As the intensity is increased, this ratio decreases to the point where the yield to the $^2P_{1/2}$ core is less than one-third that to the $^2P_{3/2}$ core. This can be quantitatively described by the shift of resonance C as described in Sec. III C.

The total yield to the different ionic ground states is plotted as a function of peak laser intensity in Fig. 12. The solid curve through the data corresponding to the $^2P_{1/2}$ core is calculated from Eq. (4) using the four-photon cross section given in Table I. The yield to the $^2P_{1/2}$ core remains nonresonant over the entire range of intensities considered. The solid curve associated with electron yield to the $^2P_{3/2}$ core is described in Sec. III C. The appearance of the electron yield in this figure also explains why the total ion yield in Fig. 7(b) is well described by an ionization rate increasing as I_0^4. First, ionization to the $^2P_{3/2}$ core does not begin to become significant until the intensity is increased to near saturation levels. Second, the nonlinearity of ionization to the $^2P_{3/2}$ core state, although increasing with intensity, does not differ significantly from $K=4$ until the ionization probability has already saturated.

The fact that at low intensities, ionization to the $^2P_{1/2}$ core of Kr^+ is strongly favored, when statistical weighting would favor the $^2P_{3/2}$ is not completely understood at this time. The behavior is reminiscent of single-photon processes where the photoionization cross sections usually fall off rapidly with excess energy above the ionization

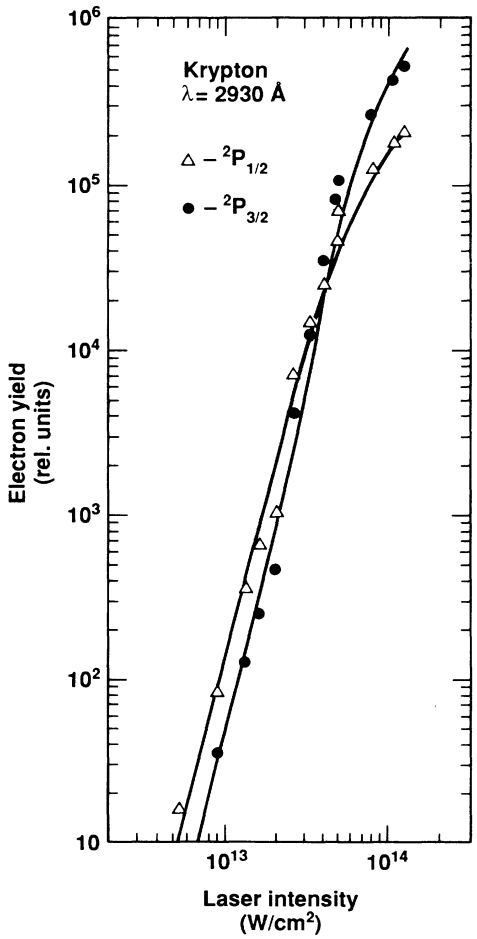

FIG. 12. Total electron yield to the $^2P_{1/2}$ and $^2P_{3/2}$ ground states of Kr^+ as a function of peak laser intensity at a laser wavelength of 293 nm. The solid curves represent the calculated electron yield as described in the text.

threshold. In the case here, the four-photon energy at 293 nm is initially 2.25 and 2.92 eV above the $P_{1/2}$ and $P_{3/2}$ ionization thresholds, respectively. This behavior could also be the result of large contributions to the four-photon matrix element by members of the $4p^5 4d'$ manifold near 104 000 cm^{-1}.

This observation is in contrast to the results of Agostini *et al.*,[46] who recorded the electron spectra resulting from the six-photon ionization of Xe at 532 nm. Their study indicated that the Xe^+ ion was left only in the $^2P_{3/2}$ final state. However, Lompre *et al.*,[47] in a more recent experiment on the multiphoton ionization of Xe at 532 nm, have observed both core states with approximately equal probability.

In all of these experiments, the relative yield to the different core states is quite different from that seen in single-photon ionization. In the case of Xe, single photons with an energy just above the $P_{1/2}$ threshold produce two bunches of electrons with a branching ratio of $\approx 1.6{:}1$. The branching ratio dips to 1.4:1 at 30 eV but eventually approaches the statistical 2:1 above 60 eV.[48]

The observation of an intensity-dependent branching ratio is not surprising in light of the field-induced shifts of the atomic energy levels and continuum. These effects may explain the different observations in the experiments of Agostini *et al.* and Lompre *et al.* on the multiphoton ionization of xenon at 532 nm. Although the experiments were similar, the difference in laser intensities could be responsible for detection of electrons corresponding to a $P_{1/2}$ core in one case but not in the other.

C. Three-photon resonant, four-photon ionization of krypton

The increase in the shift and width of the resonance apparent in Fig. 10 with increasing laser intensity is expected on the basis of the intensity dependence of field-induced shifts and the photoionization lifetime of the excited state. A surprising feature of the data is that the locations of *all* of the observed resonances shift towards higher energy. Initially, such an observation suggests that the shift of the resonances may be dominated by the ac Stark shift of the ground atomic state. This follows from the fact that for photon energies less than the energy of the first excited state, the ground state is always lowered in energy by the field.

The ac Stark shift of the ground state may be determined from knowledge of the refractive index of the material at the laser wavelength.[49] Using the experimental values of Leonard for the refractive index,[50] the dynamic Stark shifts of the ground state were calculated from 285 to 310 nm over a range of laser intensity from 5×10^{11} to 1×10^{14} W/cm^2. As an example, the calculated value of the ac Stark of the ground state of krypton at 300 nm and 10^{13} W/cm^2 was only 35 meV. Although this value is too low to quantitatively explain the observed shifts of the resonance positions, it is certainly not negligible and must be included in any calculation.

The excited states of course also experience field-induced shifts. Due to the generally larger polarizability of the excited atom, the shifts of the excited states are often much larger than that of the ground state. Calculation of the shift of the excited states is much more complicated than that of the ground state, owing to interference between the multitude of dipole-allowed pathways.

The Stark shifts of the excited states under consideration were calculated using second-order perturbation theory.[51] It was found that for the range of laser wavelengths considered in these experiments, the levels of interest should indeed *all* be shifted towards higher energy by the field. Therefore the observed "universal" blue shift can be explained within the framework of perturbation theory.

In principle, direct measurements of the shift and photoionization rate of the accessible intermediate states can be obtained by measuring the energy spectra of photoelectrons produced by resonantly enhanced multiphoton ionization with a short laser pulse.[29] This technique was not applicable for the experimental conditions here.

The shift and photoionization rate of the excited states was determined in these experiments by making quantitative measurements of the resonance profile of the ion yield as a function of laser intensity. The shift and photoionization rate can be extracted from these measure-

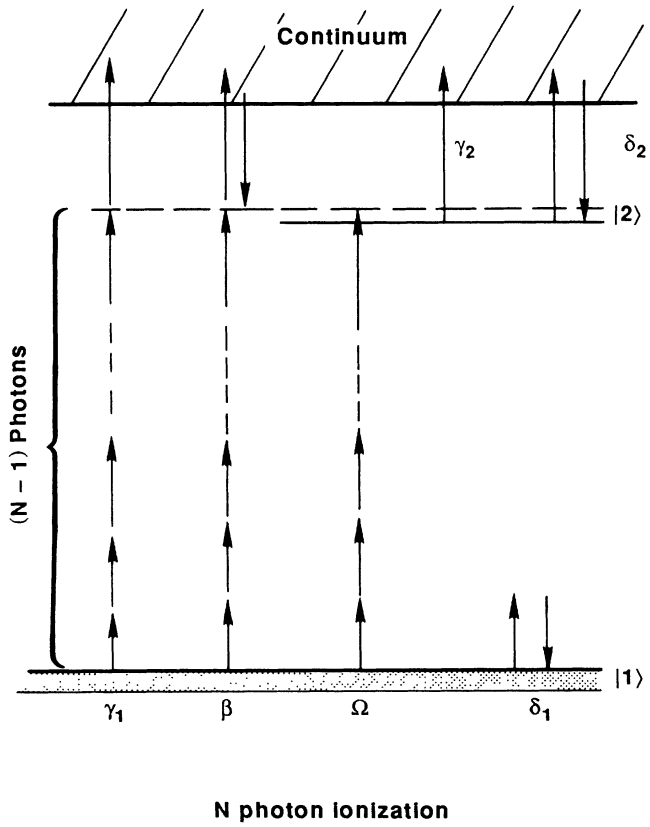

FIG. 13. Representative energy-level diagram of model atom. The multiphoton Rabi rate Ω describes the general rate of excitation from the ground to the excited state via the absorption of $N-1$ photons. β represents the excitation rate of $|2\rangle$ via the continuum. γ_1 represents nonresonant ionization, and γ_2 is the photoionization rate of the excited state. δ_1 and δ_2 are the ac Stark shifts of the ground and excited states, respectively.

ments, provided a theoretical expression for the resonantly enhanced ionization rate and the distribution of intensities over which the ions are produced are known.

An expression for the ionization rate was obtained from a model which treats the atom as being composed of only two effective bound states and the continuum (Fig. 13).[52,53] Application of the model to situations where several levels of comparable strength are near resonant may be inappropriate due to interference. The model accounts for the ac Stark shifts of both the ground δ_1 and excited state δ_2. In its most general form, nonresonant multiphoton ionization directly from the ground state and Raman-type processes resulting in population of the excited state are included. The Schrödinger equation for this system can be written

$$-\frac{\hbar}{i}\frac{\partial|\Psi\rangle}{\partial t}=\begin{bmatrix}E_1+\delta_1-i(\gamma_{1/2}) & -(\Omega+i\beta)/2\\ -(\Omega+i\beta)/2 & E_2+\delta_2-i(\gamma_{2/2})\end{bmatrix}|\Psi\rangle, \tag{7}$$

where E_1 and E_2 are the energies of the ground and excited states in the absence of the applied field, respectively. The photoionization rates of the ground state and the excited state are γ_1 and γ_2, respectively, and are functions of the local laser intensity as is the multiphoton Rabi rate Ω and the nonlinear parameter β. The effect of the multiphoton absorption on the radiation field is neglected. The bound wave function $\Psi(t)$ is written as a time-dependent expansion in the eigenfunctions of the two unperturbed states $|1\rangle$ and $|2\rangle$,

$$\Psi(t)=a_1(t)|1\rangle+a_2(t)|2\rangle\ . \tag{8}$$

The ionization probability $C(t)$ is simply the probability that the system is not in either the ground or excited state,

$$C(t)=1-|a_1(t)|^2-|a_2(t)|^2\ . \tag{9}$$

The ionization rate $W(t)$ is defined as the time derivative of the ionization probability, and may be written [using Eq. (7)] as

$$W(t)=\frac{dC}{dt}=\gamma_1|a_1(t)|^2+\gamma_2|a_2(t)|^2 +\beta(a_1a_2^*+a_2a_1^*)\ . \tag{10}$$

This expression has an important physical interpretation. The first term represents the nonresonant multiphoton ionization rate out of the ground state, while the second represents the resonantly enhanced contribution proceeding via $|2\rangle$. Each of these terms is simply the product of an ionization rate out of the state (γ_1 or γ_2, respectively) and the occupation probability of that state. The third term is more complicated as it involves mixing with the continuum. However, except for very high-field strengths, this term is small relative to the first two terms.

Equation (7) is solved exactly by assuming that the laser pulse is turned on adiabatically.[52,53] An analysis of the complete solution may be found in Ref. 52. Here, only the case where the nonresonant ionization rate is much less than the rate through the resonant intermediate state will be considered ($\gamma_1 \ll \gamma_2$).

Having determined an expression for the ionization rate, the total number of ions produced is obtained by integrating the rate equations over the spatial and temporal distribution of the laser pulse,

$$N(\omega,I_0)=\int_{-\infty}^{\infty} n_0(\mathbf{r},-\infty)\left[1-\exp\left[-\int_{-\infty}^{\infty} W[I(\mathbf{r},t),\omega,t)]dt\right]\right]d^3\mathbf{r}\ , \tag{11}$$

where $n_0(\mathbf{r},-\infty)$ is the initial target density at the point $\mathbf{r}$.

For the case of three-photon resonant, four-photon ionization of krypton, the three-photon Rabi frequency between the ground and excited states, Ω, is much less than the photoionization rate of the excited state, γ_2. With the laser intensity sufficiently high to saturate the ionization of the excited state ($\gamma_2 T_p \gg 1$), the ionization rate through the resonant pathway reduces to a simple expression,

$$W(\omega,I)=\frac{\Omega^2}{4}\frac{\gamma_2}{(3\omega-\omega_0-\alpha_s I)^2+(\gamma_2/2)^2}\ , \tag{12}$$

where α_s is the quadratic ac Stark coefficient ($\delta_1+\delta_2=\alpha_s I$) and ω_0 is the transition frequency between the ground and excited states in the limit of no applied field. For the experiments considered here, ionization of the excited state requires only a single photon and can be described by $\gamma_2=\sigma I$. The expression for the ionization rate given in Eq. (12) is valid only in the limit that the ionization rate through the resonant pathway is much larger than the nonresonant rate directly from the ground state. When the rates are comparable, the more general expressions of the model must be used.

Given the dependence of the three-photon Rabi rate on laser intensity, the ionization rate given above may be substituted into Eq. (11) to determine the total number of ions produced. We have used the perturbation-theory result for the three-photon Rabi frequency between the states $|i\rangle$ and $|m\rangle$,

$$|\Omega_{im}^{(3)}|^2=(2\pi\alpha\omega)^2|M_{im}^{(3)}(\omega)|^2I^3\ , \tag{13}$$

where α is the fine-structure constant. We define a frequency-dependent proportionality constant $\alpha(\omega)_{\text{Rabi}}$ such that $\Omega^2=\alpha(\omega)_{\text{Rabi}}I^3$.

The number of ions produced is therefore not only a function of the laser frequency and intensity but also of the internal atomic structure characterized by the parameters $\alpha_{\text{Rabi}}, \alpha_s$ and the photoionization cross section σ. Since there are three atomic parameters, three separate measurements are required to determine their values uniquely. This was accomplished by performing detailed

measurements of the spectral profiles, determination of the absolute number of ions produced as a function of laser intensity, and measuring the shift of the resonance as a function of intensity.

The results of the model calculations are presented in Figs. 12 and 14–16 along with spectral profiles of the resonances identified as the $4d'[\frac{5}{2}]_3$ and the $4d[\frac{3}{2}]_1$ respectively. The solid curve in Fig. 12, associated with electron yield to the $^2P_{3/2}$ core, is the result of model calculations for ionization through the $4d[\frac{3}{2}]_1$ intermediate state as a function of peak laser intensity at a fixed laser wavelength of 293 nm. The influence of the intermediate state being shifted into resonance at an intensity of approximately 1.5×10^{13} W/cm^2 is clearly observable as a change in the slope of the yield curve. As the intensity is increased further, the resonant enhancement becomes strong, pushing the yield to the $P_{3/2}$ core state above that to the $P_{1/2}$ state and increasing the nonlinear order from the nonresonant value of 4. At an intensity of approximately 4.5×10^{13} W/cm^2, both the nonresonant ionization to the $P_{1/2}$ and the resonantly enhanced ionization to the $P_{3/2}$ saturate. Electron yield above this intensity then comes merely from the expanding focal volume which grows as $I_0^{3/2}$.

Figures 14 and 15 show detailed spectral profiles of resonances B and C along with the results of the model calculations. The solid curve in Fig. 16 shows the results of these model calculations for the ion yield via the $4d'[\frac{5}{2}]_3$ as a function of intensity at 288.5 nm. The atomic parameters α_s, α_{Rabi}, and σ were varied until the unique combination representing the "best" fit to the experimental data was obtained. All other parameters (e.g., target density, laser pulse width, etc.) were held fixed at their experimentally determined values. The values of the atomic parameters are given in Table II.

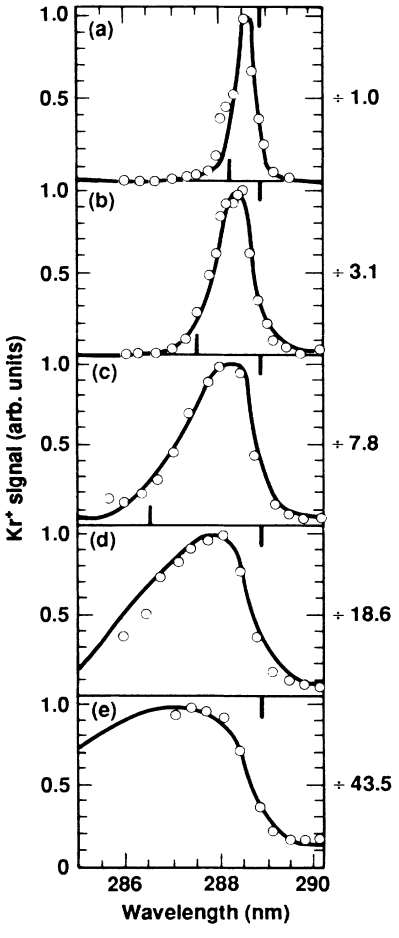

FIG. 14. Spectral profile of resonance B, attributed primarily to the $4d'[\frac{5}{2}]_3$, for various peak intensities: (a) $I_0=7.4\times10^{12}$ W/cm^2, (b) $I_0=1.5\times10^{13}$ W/cm^2, (c) $I_0=2.7\times10^{13}$ W/cm^2, (d) $I_0=4.5\times10^{13}$ W/cm^2, (e) $I_0=7.8\times10^{13}$ W/cm^2. Solid curves are the result of model calculations as described in the text.

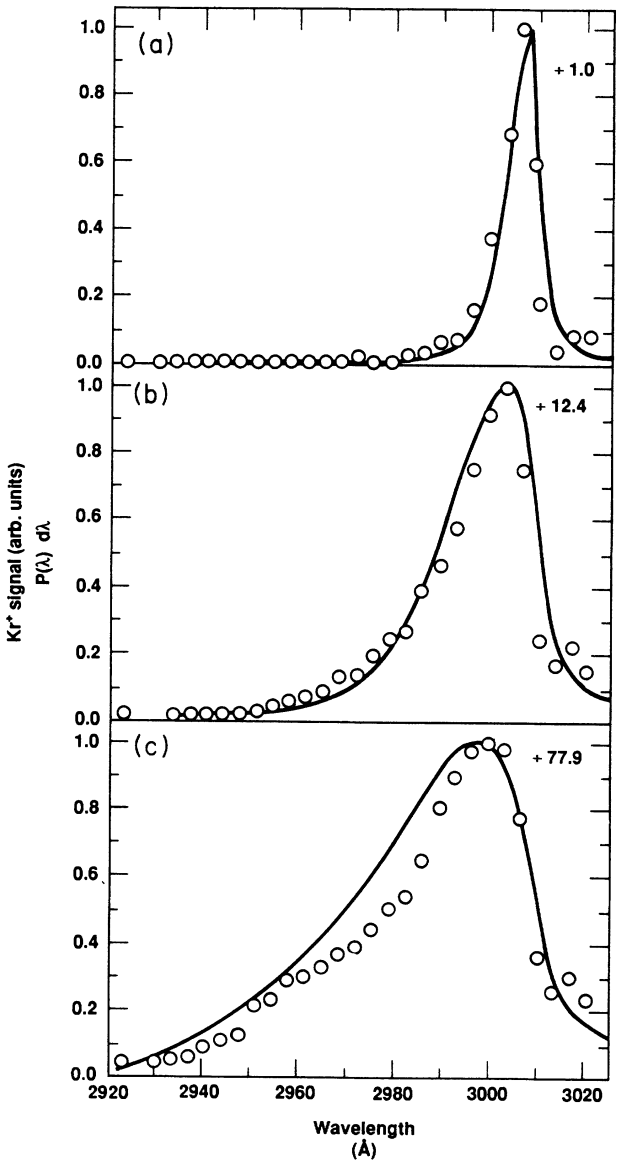

FIG. 15. Spectral profile of resonance C for various peak intensities: (a) $I_0=5.8\times10^{12}$ W/cm^2, (b) $I_0=1.4\times10^{13}$ W/cm^2, (c) $I_0=2.8\times10^{13}$ W/cm^2. Solid curves are the results of model calculations as described in the text.

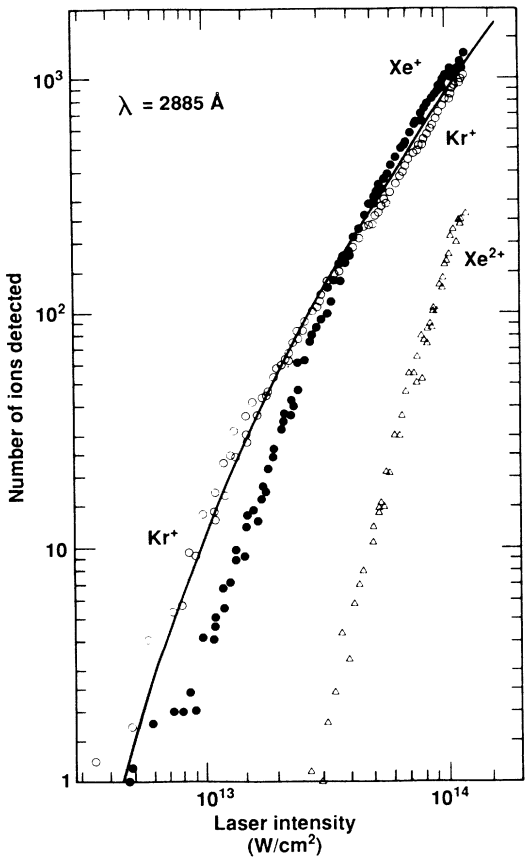

FIG. 16. Absolute yield of Kr^+ at 288.5 nm as a function of peak intensity. The solid curve is the result of model calculations using the parameters given in Table II.

The quality of the agreement between the model calculations and the experimental data is surprisingly good considering the high-field strengths involved. The asymmetric profile of Figs. 14 and 15 is a direct result of the distribution of intensity characteristic of a realistic laser pulse. The intensity distribution results in a distribution of Stark shifts throughout the focal volume. Hence atoms at different locations exhibit different resonance frequencies.

The effect of saturation can also be seen at the higher intensities and is quite pronounced in the case of the $4d[\frac{3}{2}]_1$. Saturation occurs when the laser intensity is high enough that $\Omega^2 T_p/\gamma_2$ approaches or exceeds unity. Saturation further distorts the already asymmetric resonance profile. This is a result of the depletion of target

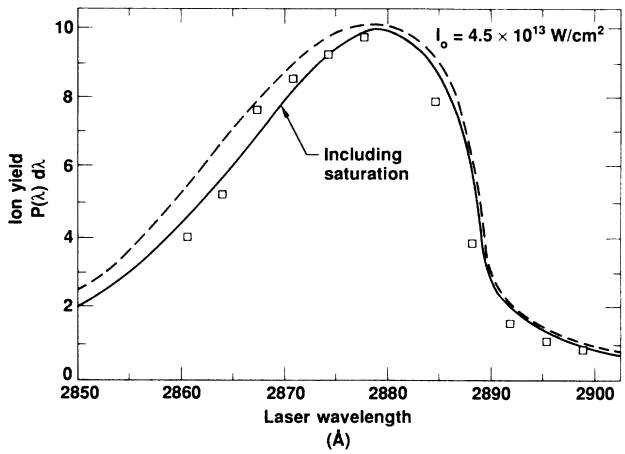

FIG. 17. Spectral profile of resonance B at a peak intensity of 4.5×10^{13} W/cm^2. The solid curve is the result of model calculations which include saturation of the ionization probability.

atoms in the volume experiencing the highest intensities. As these are the atoms experiencing the largest field-induced shifts, the spectral profile will become further depressed in the regions of the largest shifts near saturation. This behavior is illustrated in Fig. 17 for resonance B which shows a comparison of ion yields calculated from Eq. (11) (saturation included) and a first-order expansion of Eq. (11) (saturation neglected).

The appearance of electrons corresponding to both ionic core states resulting from three-photon resonant, four-photon ionization of Kr near 288.5 nm (Fig. 3) is interpreted as evidence that the $4p^5 4d'[\frac{5}{2}]_3$ state is not a pure configuration. This has been suggested previously by Aymar and Coulombe.[43] Contribution from the nearby $5d[\frac{1}{2}]_1$ state can be examined by measuring the yield of the photoelectrons as a function of laser polarization. These experiments are currently in progress.

The identification of resonance C was further investigated by measuring the ion yield near 300 nm using both linearly and circularly polarized light. At low intensity, the ion yield using linearly polarized light was more than a factor of 10 larger than the yield observed using circularly polarized light. This ratio decreased to slightly more than a factor of 3 near the saturation intensity. Nevertheless, the enhancement in the ion yield was clearly due to resonance with intermediate states which are accessible with linearly but not circularly polarized light. This is in agreement with the initial identification of resonance C as being a mixture of the $4d[\frac{3}{2}]_1$ and the $6s[\frac{3}{2}]_1$.

TABLE II. Measured atomic parameters in the four-photon ionization of Kr.

Excited state (j_c 1)	Laser wavelength (nm)	Three-photon Rabi coefficient (cm^6 sec)	Net ac Stark shift (meV/TW cm^2)	Photoionization cross section (10^{18} cm^2)
$4d'[\frac{5}{2}]_3$	288–289	$(2\pm0.7)\times10^{-69}$	3.9±0.7	3.0±0.6
$4d[\frac{3}{2}]_1$	299–301	$(8\pm4)\times10^{-69}$	8.0±0.8	8±1
$H{:}2p$[a]	365	1.3×10^{-68}	7±2	13±4

[a]Reference 54.

IV. CONCLUSION

In summary, the experiments described herein have extended the intensity to 6×10^{13} W/cm^2 where resonant enhancement of the ion yield resulting from multiphoton ionization has been observed. The resonance profiles are well described by a simple model utilizing perturbation theory for the excitation and ionization rates, even when the strength of the applied laser field exceeded 5% of the atomic field strength. Absolute values of the multiphoton ionization cross section of Kr, Xe, and Xe^+ from 285 to 310 nm are reported. In addition, we have measured the three-photon excitation rate to, the ac Stark shift and the single-photon ionization cross section of selected members of the $4p^5 4d$ and $4p^5 4d'$ manifolds in Kr.

Intensity-dependent branching ratios of photoelectrons corresponding to the $^2P_{3/2}$ and $^2P_{1/2}$ core states have been observed and are quantitatively explained by influence of intermediate states shifted by the intense field. Accurate calibration of the local laser intensity was obtained by measuring the ponderomotive energy shift of photoelectrons resulting from the multiphoton ionization of krypton with short laser pulses. This technique was also used as an alternative method for determination of the saturation intensity in nonresonant multiphoton ionization.

In view of the recent success of theories which include tunneling ionization in explaining experiments conducted at similar intensities in the visible region of the spectrum,[32,55] the ability of perturbation theory to describe these results may seem surprising.

As first suggested by Keldysh,[39] the contribution of tunneling to the ionization rate can be estimated by calculation of a parameter γ which is defined as the ratio of the frequency of the applied laser field to the tunneling frequency. This parameter can also be written as the square root of the ratio of the field-free ionization potential to twice the ponderomotive potential, $\gamma=[I_p(0)/2U_p]^{1/2}$. The limit $\gamma\gg1$ is identified with conventional multiphoton ionization where lowest-order perturbation theory is expected to provide an adequate description. In the limit that $\gamma\ll1$, tunneling is expected to dominate the ionization mechanism. This region is characterized by an ionization rate which increases with intensity more slowly than that predicted by perturbation theory and is dominated by above-threshold ionization.

These experiments cover a region of $2<\gamma<10$ and therefore can be considered to lie in an intermediate regime. This is confirmed by the data of Fig. 8 in that above-threshold ionization is becoming important, signifying the breakdown of lowest-order perturbation theory. However, calculations by Szöke[56] suggest that the intensity dependence of the ionization rate predicted by an extended Keldysh-Reiss-Faisal theory[32,57,58] for these experimental conditions does not differ significantly from that described by perturbation theory. This is confirmed by the calculations of Kulander.[18]

ACKNOWLEDGMENTS

We would like to thank A. Szöke and E. M. Campbell for many helpful discussions and for reading this manuscript. We also thank A. Szöke and R. Shelton for their assistance with the electron spectrometer. This work was supported by the Institutional Research and Development program at the Lawrence Livermore National Laboratory and performed under the auspices of the U. S. Department of Energy Contract No. W-7405-ENG-48.

[1] J. Morellec, D. Normand, and G. Petite, Phys. Rev. A **14**, 300 (1976); G. Petite, J. Morellec, and D. Normand, J. Phys. (Paris), Colloq. **40**, 115 (1979).

[2] L. A. Lompre, G. Mainfray, C. Manus, and J. Thebault, Phys. Rev. A **15**, 1604 (1977); L. A. Lompre, G. Mainfray, and C. Manus, J. Phys. B **13**, 85 (1980); L. A. Lompre, G. Mainfray, C. Manus, and J. D. Marinier, *ibid.* **14**, 4307 (1981).

[3] G. C. Bjorklund, R. R. Freeman, and R. H. Storz, Opt. Commun. **31**, 47 (1979).

[4] R. N. Compton, J. C. Miller, A. E. Carter, and P. Kruit, Chem. Phys. Lett. **71**, 87 (1980).

[5] J. Bokor, J. Zavelovich, and C. K. Rhodes, Phys. Rev. A **21**, 1453 (1980).

[6] U. Eichmann, Y. Zhu, and T. F. Gallagher, J. Phys. B **20**, 4461 (1987).

[7] A. T. Georges and P. Lambropoulos, Phys. Rev. A **15**, 727 (1977); Adv. Electron. Electron Phys. **54**, 191 (1980).

[8] Y. Gontier and M. Trahin, J. Phys. B **13**, 259 (1980).

[9] P. Zoller, J. Phys. B **15**, 2911 (1982).

[10] M. Crance, J. Phys. B **13**, 101 (1980).

[11] F. H. M. Faisal, R. Wallenstein, and H. Zacharias, Phys. Rev. Lett. **39**, 1138 (1977).

[12] P. Kruit, J. Kimman, H. G. Muller, and M. J. van der Wiel, J. Phys. B **16**, 937 (1983).

[13] See F. H. M. Faisal, *Theory of Multiphoton Processes* (Plenum, New York, 1987).

[14] P. Gangopadhay, X. Tang, P. Lambropoulos, and R. Shakeshaft, Phys. Rev. A **34**, 2998 (1986).

[15] G. Mainfray and C. Manus, Appl. Opt. **19**, 3934 (1980); G. Mainfray, in *Multiphoton Ionization of Atoms,* edited by S. L. Chin and P. Lambropoulos (Academic, New York, 1984).

[16] L. A. Lompre, G. Mainfray, and C. Manus, J. Phys. B **13**, 85 (1980).

[17] R. R. Freeman, R. H. Bucksbaum, H. Milchberg, S. Darack, D. Schumacher, and M. E. Geusic, Phys. Rev. Lett. **59**, 1092 (1987).

[18] K. C. Kulander, Phys. Rev. A **38**, 778 (1988).

[19] M. D. Perry, O. L. Landen, and A. Szöke (unpublished).

[20] A. L'Hullier, L. A. Lompre, G. Mainfray, and C. Manus, J. Phys. B **16**, 1363 (1983); Phys. Rev. A **27**, 2503 (1983).

[21] M. D. Perry, O. L. Landen, A. Szöke, and E. M. Campbell, Phys. Rev. A **37**, 747 (1988).

[22] T. W. B. Kibble, Phys. Rev. **150**, 1060 (1966); Phys. Rev. Lett. **16**, 1054 (1966).

[23] P. Agostini, J. Kupersztych, L. A. Lompre, G. Petite, and F. Yergeau, Phys. Rev. A **36**, 4111 (1987).

[24]T. S. Luk, T. Graber, H. Jara, U. Johann, K. Boyer, and C. K. Rhodes, J. Opt. Soc. Am. B **4**, 847 (1987).
[25]M. D. Perry, UCRL Report No. 97375, 1987 (unpublished); L. Jönsson (unpublished).
[26]P. Kruit and F. H. Read, J. Phys. E **16**, 313 (1983).
[27]P. Kruit, J. Mimman, H. G. Muller, and M. J. van der Wiel, Phys. Rev. A **28**, 248 (1983); P. H. Bucksbaum, M. Bashkansky, and T. J. McIlrath, Phys. Rev. Lett. **58**, 349 (1987).
[28]M. Crance, J. Phys. B **19**, L267 (1986).
[29]A. Szöke, O. L. Landen, and M. D. Perry (unpublished).
[30]S. Pratt, P. H. Dehmer, and J. L. Dehmer, Phys. Rev. A **35**, 3793 (1987).
[31]M. R. Cervenan and N. R. Isenor, Opt. Commun. **13**, 175 (1975).
[32]M. D. Perry, A. Szöke, O. L. Landen, and E. M. Campbell, Phys. Rev. Lett. **60**, 1270 (1988).
[33]U. Johann, T. S. Luk, H. Egger, and C. K. Rhodes, Phys. Rev. A **34**, 1084 (1986).
[34]A. L'Hullier (private communication).
[35]G. Petite, P. Agostini, and F. Yergeau, J. Opt. Soc. Am. B **4**, 765 (1987).
[36]R. R. Freeman, T. J. McIlrath, P. H. Bucksbaum, and M. Bashkansky, Phys. Rev. Lett. **57**, 3156 (1986). T. J. McIlrath, P. H. Bucksbaum, R. R. Freeman, and M. Bashkansky, Phys. Rev. A **35**, 4611 (1987).
[37]P. Kruit, H. G. Muller, J. Kimman, and M. J. van der Wiel, J. Phys. B **16**, 2359 (1983).
[38]A. Szöke, J. Phys. B **18**, L427 (1986).
[39]The "multiphoton regime" is defined here as regions of laser frequency and intensity for which the tunneling parameter γ is much greater than unity. This parameter is defined in Sec. IV and in L. V. Keldysh, Zh. Eksp. Teor. Fiz. **47**, 1945 (1964) [Sov. Phys.—JETP **20**, 1307 (1965)].
[40]O. L. Landen, M. D. Perry, and E. M. Campbell, Phys. Rev. Lett. **59**, 2558 (1987).
[41]V. Kaufman and C. J. Humphreys, J. Opt. Soc. Am. **59**, 1614 (1969); C. E. Moore, *Atomic Energy Levels,* Natl. Bur. Stand. (U.S.) Circ. No. 169 (U. S. GPO, Washington, D. C., 1948), Vol. II.
[42]P. Lambropoulos, Adv. At. Mol. Phys. **12**, 87 (1976).
[43]M. Aymar and M. Coulombe, At. Data Nucl. Data Tables **21**, 537 (1978).
[44]R. N. Compton, J. C. Miller, A. E. Carter, and P. Kruit, Chem. Phys. Lett. **71**, 87 (1980).
[45]K. Sato, Y. Achiba, and K. Kimura, J. Chem. Phys. **80**, 57 (1983).
[46]P. Agostini, F. Fabre, G. Mainfray, G. Petite, and N. K. Rahman, Phys. Rev. Lett. **42**, 1127 (1979).
[47]L. A. Lompre, G. Mainfray, C. Manus, and J. Kupersztych, J. Phys. B **20**, 1009 (1987).
[48]F. Wuilleumier, M. Y. Adam, P. Dhez, N. Sandner, V. Schmidt, and W. Mehlhorn, Phys. Rev. A **16**, 646 (1977).
[49]J. D. Jackson, *Classical Electrodynamics,* 2nd ed. (Wiley, New York, 1975).
[50]P. J. Leonard, At. Data Nucl. Data Tables **14**, 21 (1974).
[51]A. M. Bonch-Bruevich and U. A. Khodovor, Usp. Fiz. Nauk **10**, 71 (1967) [Sov. Phys.—Usp. **93**, 637 (1967)].
[52]M. D. Perry, Ph. D. thesis, University of California, Berkeley, 1988.
[53]C. R. Holt, M. G. Raymer, and W. P. Reinhardt, Phys. Rev. A **27**, 2971 (1983); L. Allen and J. H. Eberly, *Optical Resonance and Two-Level Atoms* (Wiley, New York, 1975).
[54]D. E. Kelleher, M. Ligare, and L. R. Brewer, Phys. Rev. A **31**, 2747 (1985).
[55]P. B. Corkum (unpublished).
[56]A. Szöke (private communication).
[57]F. H. M. Faisal, J. Phys. B **6**, 189 (1973).
[58]H. R. Reiss, Phys. Rev. A **22**, 1786 (1980).

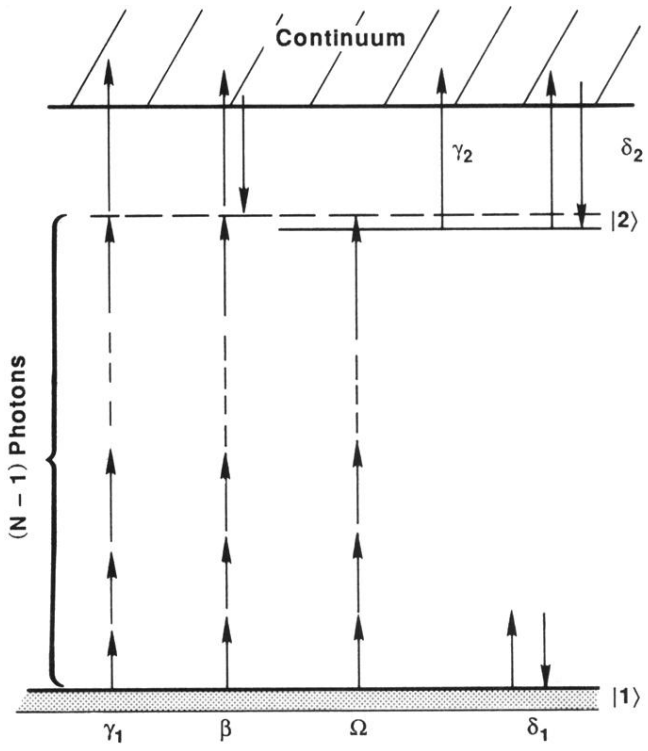

FIG. 13. Representative energy-level diagram of model atom. The multiphoton Rabi rate Ω describes the general rate of excitation from the ground to the excited state via the absorption of $N-1$ photons. β represents the excitation rate of $|2\rangle$ via the continuum. γ_1 represents nonresonant ionization, and γ_2 is the photoionization rate of the excited state. δ_1 and δ_2 are the ac Stark shifts of the ground and excited states, respectively.